



# Advanced Microfluidic Platform for Tumor Spheroid Formation and Cultivation Fabricated from OSTE+ Polymer

Petr Panuška<sup>1</sup> · Jiří Smejkal<sup>1</sup> · Marcel Štofík<sup>1</sup> · Zuzana Žmudová<sup>1</sup> · Klára Španbauerová<sup>1</sup> · Jaromír Havlica<sup>2,3</sup> · Václav Harrandt<sup>2,3</sup> · Stanislav Vinopal<sup>1</sup> · Petr Aubrecht<sup>1</sup> · Jan Malý<sup>1</sup>

Received: 23 January 2024 / Revised: 31 May 2024 / Accepted: 16 July 2024 / Published online: 30 July 2024  
© The Author(s) 2024

## Abstract

In the evolving landscape of cancer research, 3D cell cultures, particularly tumor cell spheroids, are increasingly preferred in drug screening due to their enhanced mimicry of *in vivo* tumor environments, especially in drug resistance aspects. However, the consistent formation of uniform spheroids and their precise manipulation remain complex challenges. Among various methodologies, droplet microfluidics emerges as a highly effective approach for tumor spheroid formation. This paper introduces a novel, multifaceted microfluidic system that streamlines the entire spheroid cultivation process: (i) generating tumor spheroids from cell suspensions within individual droplets, (ii) merging these droplets into a continuous aqueous phase once spheroid formation is complete, and (iii) transferring the spheroids to a specialized cultivation area within the chip, equipped with trapping elements for extended cultivation in perfusion mode. Remarkably, this process requires no hydrogel encapsulation or external handling, as all operations are conducted within the microfluidic chip. Fabricated from the innovative OSTE+ (off-stoichiometry thiol-ene epoxy) polymer, the chip is designed for repeated use. To show its efficacy, we successfully formed spheroids from MCF-7, GAMG, and U87 cell lines in our system and compared them with spheroids prepared by a traditional agarose microwell method. Additionally, our methodology has successfully enabled the in-chip release of spheroids from droplets, followed by their effective trapping for subsequent cultivation, a process we have exemplified with MCF-7 spheroids. To our knowledge, this research represents the first instance of a fully integrated droplet microfluidic platform achieving scaffoldless tumor spheroid formation and handling. Our method holds promise for improving high-throughput, automated procedures in the formation, transfer, and cultivation of tumor cell spheroids.

---

✉ Petr Panuška  
petr.panuska@ujep.cz

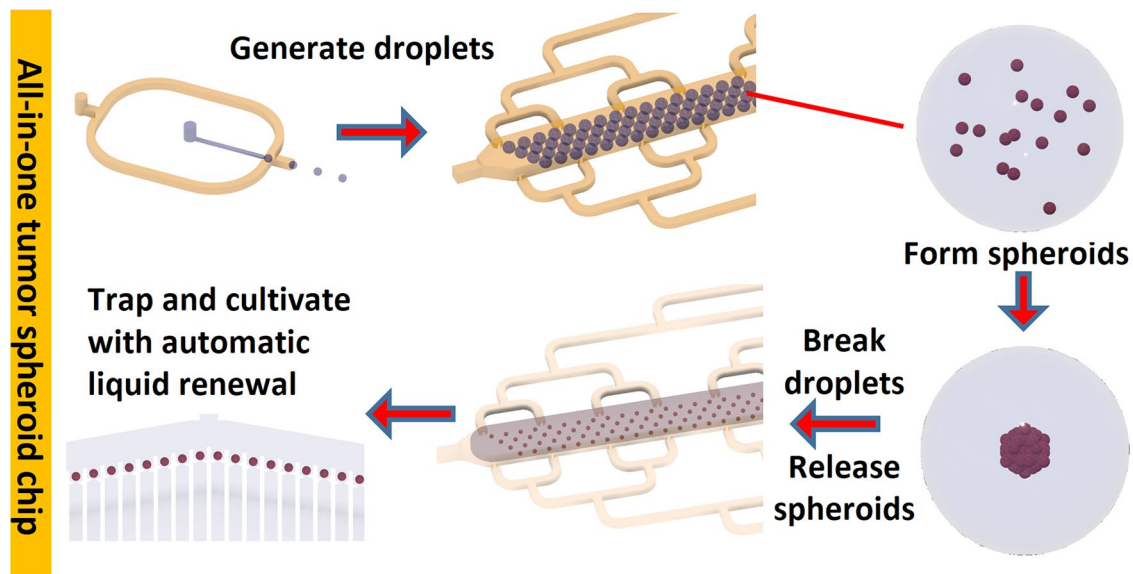
✉ Jan Malý  
jan.maly@ujep.cz

<sup>1</sup> CENAB, Faculty of Science, Jan Evangelista Purkyně University in Ústí nad Labem, Pasteurova 3632/15, 400 96 Ústí nad Labem, Czech Republic

<sup>2</sup> Department of Chemistry, Faculty of Science, Jan Evangelista Purkyně University in Ústí nad Labem, Pasteurova 3632/15, 400 96 Ústí nad Labem, Czech Republic

<sup>3</sup> Institute of Chemical Process Fundamentals, The Czech Academy of Sciences, Rozvojova 2/135, 165 02 Prague, Czech Republic

## Graphical abstract



**Keywords** Droplet microfluidics · 3D tumor spheroids · OSTC+ polymers · Spheroid cultivation · Microfluidic spheroid traps

## 1 Introduction

Cancer continues to be a leading cause of death, often progressing asymptotically and leading to metastases that are challenging to cure with current methods [1–3]. As new anticancer drugs are developed, the need for accurate and easily obtainable tumor models is critical. Traditional 2D cell cultures, once standard for *in vitro* testing, have been found inadequate in simulating real tumors, especially concerning drug resistance and cell communication [4]. In recent decades, 3D cell cultures have gained prominence as more representative tumor models. These cultures, by incorporating the extracellular matrix (ECM), better mimic *in vivo* tumors in drug screening [2], displaying enhanced resistance and more tumor-like gene expression and physiological responses [4].

Spheroid formation, a pivotal aspect in tumor model research, can be achieved through various methods, either scaffold-based (using support structures from different materials) or scaffold-free. Prominent techniques include pellet culture, spinner culture, hanging drop, liquid overlay on non-adherent surfaces, and approaches leveraging external forces like magnetic/electric fields and ultrasound. Additionally, microfluidic and hydrogel-based methods are widely recognized. Each of these methods has its unique pros and cons, extensively documented in literature [5, 6]. Notably, these approaches can be integrated, particularly in microfluidics, enhancing their applicability. Specifically,

microfluidics in spheroid formation and manipulation shows promise for the development of high-throughput, automated systems vital for large-scale drug screening and other applications. Particularly notable is the droplet microfluidic technique, which is often enhanced through the integration of hydrogels for encapsulating spheroids, as evidenced in several studies [7–10].

Numerous droplet-based microfluidic chips for spheroid generation and cultivation have been developed, mostly using PDMS, glass, or their combinations. Yu et al. [11] created a chip for hydrogel-encapsulated spheroid formation, taking four days for spheroid formation and subsequent drug testing. Yoon et al. [12] developed a chip for cell encapsulation with magnetic nanoparticles in alginate hydrogel, facilitating spheroid transfer using magnetic force but lacking in-chip cultivation. In 2015, Kim et al. [7] highlighted the challenge of cell quantity regulation in alginate hydrogel droplets for uniform spheroid size, proposing an improved microfluidic platform. Sabhachandani et al. [13] created a platform for trapping spheroids from multiple cell types in alginate hydrogel, enabling medium perfusion and drug testing, despite the irregular spheroid shape. Cui et al. [8] introduced a thermoresponsive hydrogel-based droplet microfluidic platform for easier spheroid harvesting. Kwak et al. [14] reported a system for uniform spheroid formation from MCF-7 and MDA-MB-231 cells, requiring post-chip processing for spheroid cultivation. Sun et al. [10] developed a chip for co-culture tumor spheroids in

core–shell alginate hydrogel droplets, performing drug tests off-chip. Liu et al. [9] showed droplet generation without oil using hydrogels, focusing on rat pancreatic islet cells. De Lora et al. [15] created an oil-free acoustofluidic droplet chip using hydrogels, leveraging acoustic waves for droplet generation. Lee et al. [16] developed a system for rapid droplet generation and adjustable spheroid size, using brain tumor cells for phototherapy tests. Wu et al. [17] fabricated a chip for breast tumor spheroids with matrigel, enabling quick formation and drug testing. Zhang et al. [18] designed a platform for hydrogel-encapsulated tumor spheroids, transferring droplets to microwell plates for cultivation.

Previous solutions for tumor spheroid generation in microfluidics, mentioned above, typically fell into two categories: those designed for creating spheroids from cell suspensions for external handling post-formation [7, 8, 10–12, 15–18], and those utilizing hydrogels for spheroid encapsulation and in-chip handling [7–13, 17, 18]. Hydrogel often extended spheroid formation time (up to 4 days) [12, 13] and yielded smaller spheroids with irregular structures [7, 8, 10–13]. Handling spheroids outside the chip can be challenging, potentially causing mechanical stress that affects the model's quality. Additionally, hydrogel-supported spheroids may not accurately mimic the natural tumor microenvironment, thus limiting the biological relevance of the model.

Addressing the limitations of existing microfluidic technologies, our research was focused on refining the droplet microfluidic approach for generating uniform, scaffoldless 3D cell cultures (spheroids), with an emphasis on complete in-chip handling. We developed a microfluidic chip comprising integrated droplet generator, reservoir, and cultivation sections, functioning as an integrated system. This design enabled the formation of spheroids from three distinct cancer cell lines (MCF-7, GAMG, and U87) within aqueous droplets, followed by in-chip droplet coalescence and subsequent transfer of spheroids to the chip's trapping/cultivation section for additional processing. We also explored the use of a novel material, OSTE+ polymer (off-stoichiometry thiol-ene epoxy) [19–22], for chip fabrication, offering several advantages over traditional PDMS, which could not be used for such purpose. The use of OSTE+ polymer was necessary mainly due to its resistance to the oil phase and necessity to introduce different surface modifications/properties in some parts of the chip based on their different functionality. Further on, the technical solution of droplet coalescence channels and hydrodynamic solution of a cultivation part enabling the automatic immobilization of spheroids in chambers with low probability of non-homogenous distribution was proposed and tested with success.

To the best of our knowledge, this study is the first to accomplish all necessary steps for scaffoldless tumor

spheroid formation and cultivation within a fully integrated droplet microfluidic platform. We also discuss the potential of this innovative approach for advancing high-throughput, automated methods for the formation, transfer and cultivation of cancer spheroids.

## 2 Materials and Methods

### 2.1 Design of the Microfluidic Chip

The microfluidic chip was designed with the help of CAD (Computer-Aided Design) software Autodesk Fusion 360 (Autodesk Inc., USA). The chip can be used for the generation of aqueous phase cell suspension droplets in the high-density oil phase, coalescence of droplets with formed spheroids, and their subsequent trapping in the cultivation part. For this purpose, the chip consists of three functional parts: (i) the droplet generator, (ii) the droplet reservoir, and (iii) the spheroid cultivator (Fig. 1). The droplet generator is a microfluidic cross-junction with lateral oil phase channels of  $800 \times 800 \mu\text{m}$  square profiles and center aqueous phase channel of  $200 \times 200 \mu\text{m}$  square profile at the intersection area (Fig. 2a). These dimensions were adjusted for generation of aqueous droplets with a diameter of around  $800 \mu\text{m}$  with our specific oil phase and surfactant. The size of the droplets can be regulated, to a certain extent, by adjusting the oil and water flow rates. The droplet reservoir part provides space inside the chip where the generated aqueous droplets with cell suspension can be stored before the spheroids are formed. It contains lateral branched channels (Figs. 1 and 2a, b) that can be used to wash the content of the reservoir with any aqueous or oil phase solutions, with the main purpose of coalescing the droplets once the spheroids are formed. After coalescing the droplets, the spheroids can be transferred in the aqueous phase into the spheroid cultivation part of the chip. This part has a sieve structure (Fig. 2e) that allows the trapping of individual spheroids. The spheroids are trapped in separated chambers, with medium perfusion through each of these chambers. The design of the spheroid cultivation part and its trapping mechanism were step-by-step optimized by CFD simulations and experiments. It reflects the requirement of being able to trap the spheroids, which behave as macroscopic (relative to the molecules of the liquid) solid spheres, and the requirement to have the liquid flowing through all the trapping chambers, in the ideal case with an equal flow rate through each chamber.

### 2.2 Fabrication of the Microfluidic Chip

The chip was fabricated from off-stoichiometry thiol-ene epoxy-based polymer (OSTE+) (OSTEMER 322 Crystal Clear, Mecrene Labs AB, Sweden). To achieve the

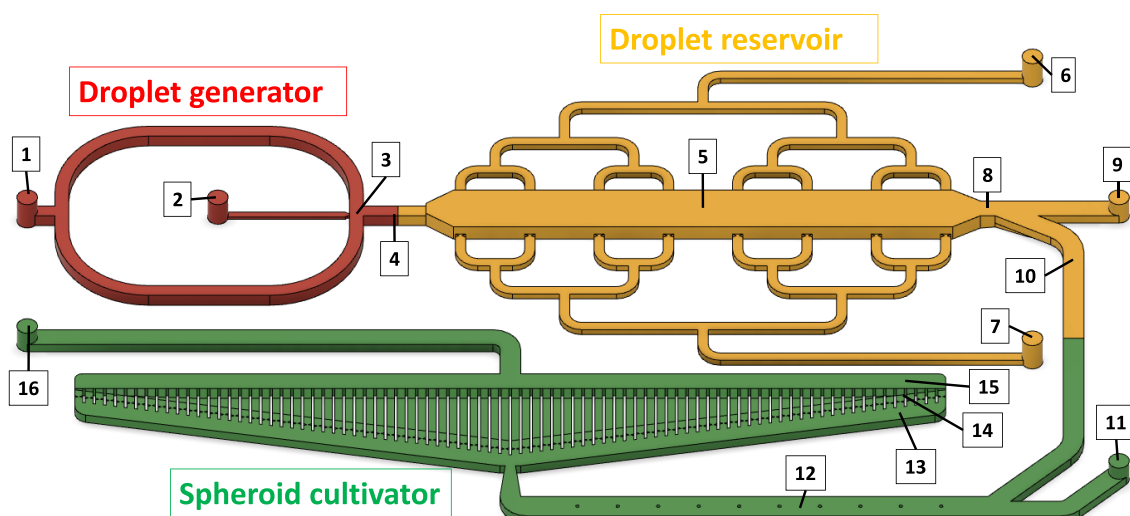


**Fig. 1** Overview of microfluidic chip design. 1-Oil phase inlet; 2-aqueous phase inlet; 3-cross-junction; 4-connecting channel between droplet generator and reservoir; 5-droplet reservoir area; 6-reservoir side channel inlet; 7-reservoir side channel outlet; 8-reservoir outlet channel; 9-reservoir outlet; 10-channel connecting drop-

let reservoir and spheroid cultivator; 11-spheroid cultivator medium inlet; 12-spheroid cultivator inlet channel; 13-spheroid cultivator inlet area; 14-spheroid cultivator trapping element area; 15-spheroid cultivator outlet area; 16-spheroid cultivator outlet

required structure from OSTE+ polymer, we first used a DLP (Digital Light Processing) 3D printer Perfactory<sup>®</sup> IV LED (Envisiontec GmbH, Germany) to create a primary, positive molding master. The material of the master was a methacrylic/acrylic based polymer HTM 140 v2 (Envisiontec GmbH, Germany). We poured vacuum-debubbled PDMS (Sylgard 184, Dow Corning, USA) 10:1 w/w base:initiator mixture into this master and incubated on a hot plate at 65 °C for 24 h, to create a secondary, negative master, which was later used for molding of the OSTE+ polymer. After pouring the OSTE+ monomer mixture into the PDMS master, bubbles were removed using vacuum, following a manual removal with a small steel spoon (to move the bubbles up to the surface) and a medical syringe (to suck the bubbles out from the surface). The master filled with the debubbled OSTE+ monomer mixture was carefully covered with a 1 mm thick glass (Corning) to remove excess liquid material, while not letting air get inside during this process. Another glass layer was put under the master, to prevent the PDMS master from deforming during handling. The OSTE+ monomer mixture was then illuminated with a UV source (1000 W, lithograph SÜSS MICROTREC SE, Germany) through the 1 mm thick glass top layer and also through a light scattering glass, which was a part of the lithograph. This scattering glass helped to prevent the OSTE+ mixture from polymerizing too quickly, which could otherwise significantly reduce its transparency. The microfluidic chip was designed to be assembled from two OSTE+ polymer parts, top and bottom. Each of these parts had its own masters and was illuminated with different UV

doses (700 mJ/cm<sup>2</sup> for the bottom part and 1100 mJ/cm<sup>2</sup> for the top part, not counting the attenuation from the glass layers). After the first curing step by UV light, the OSTE+ prepolymer parts were removed from the PDMS masters, where the bottom part was kept on the Corning glass, and the top part was separated from the glass layer. The top and bottom parts were manually aligned and put onto each other, following a second curing step of the OSTE+ prepolymer, baking it at 100 °C for 90 min in an electric oven (LAC, Czech Rep.), which caused the material to harden and covalently bonded the two parts and the glass layer together (the glass layer only served as a support, it was not in contact with any functional part of the chip). After the second cure step, a 3D printed (HTM 140 v2) interface was connected to the chip inlets and outlets, which contained UNF 1/4-28 screw threads for microfluidic connectors. The bonding of the interface to the chip was done with UV reactive glue (CONLOC UV 688, EGO Dichtstoffwerke GmbH, Germany), illuminated with 100 J/cm<sup>2</sup> UV dose. After that, the whole chip was sonicated in isopropanol for 30 min for cleaning and removal of any excess unreacted glue and then blown dry with nitrogen. Finally, the inner surface of the chip was modified with two different agents. The cultivation part was modified with Silane-PEG-OH, 1 k PEG chain (Biopharma PEG Scientific Inc., USA) by filling it with 1 µg/mL solution of the silane in acetone, while also sealing the inlets and outlets of the generator and reservoir part to prevent contamination of those parts and then putting the chip into electric oven (LAC, Czech Rep.), baking it at 100 °C for 90 min. The generator and reservoir areas were

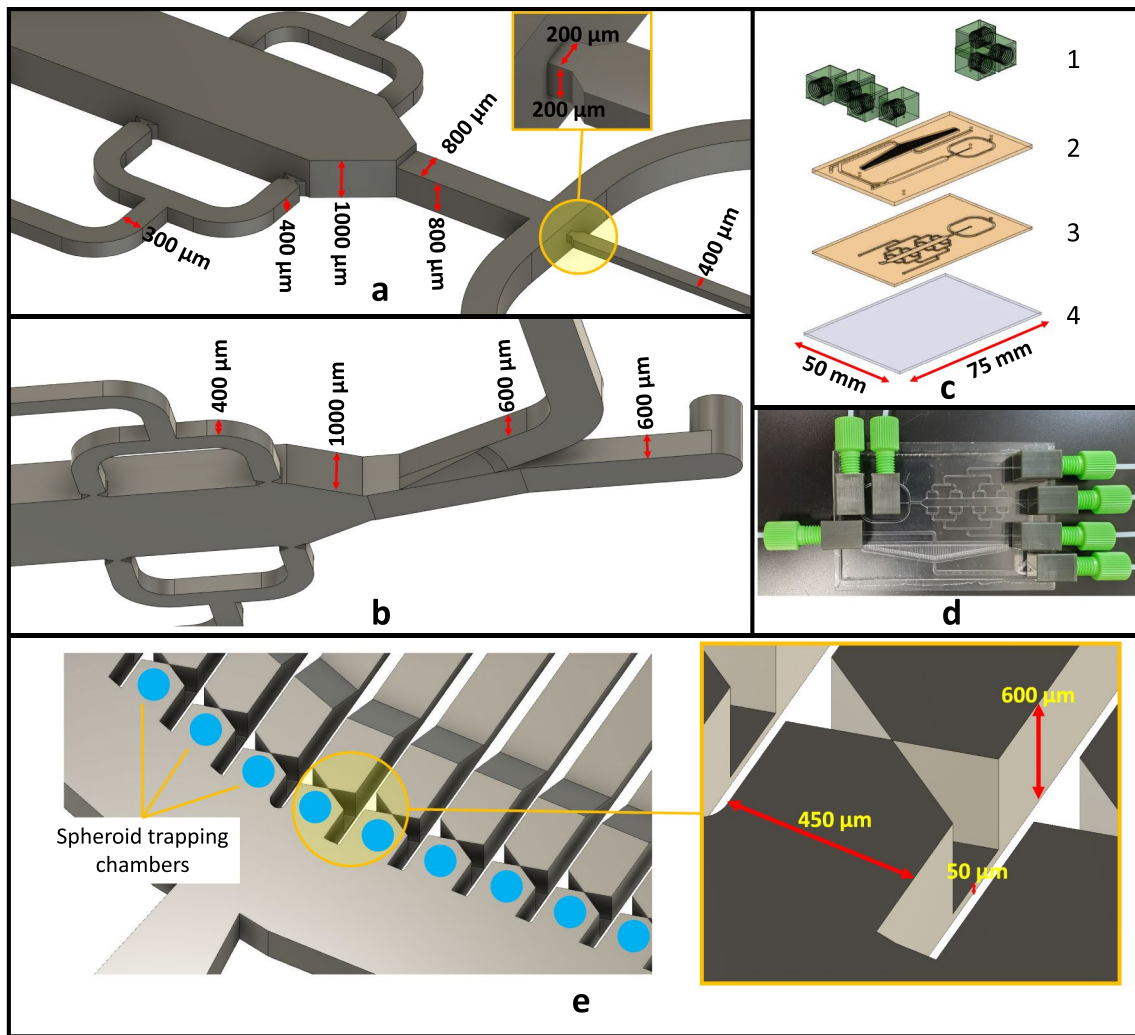


**Fig. 2** Detailed overview of functional parts of the microfluidic chip. **a** Details of the structure of the cross-junction and reservoir side branches; **b** details of the structure of the reservoir outlet with angled bottom ending; **c** CAD illustration of the separate layers of the microfluidic chip: 1-3D printed interface with threads for microfluidic fit-

tings, 2- top part from OSTE+ polymer, 3-bottom part from OSTE+ polymer, 4-glass support layer; **d** assembled microfluidic chip with connected fittings and tubing; **e** details of the spheroid cultivation part and its trapping mechanism, with a zoomed section with critical dimensions

modified with fluorosilane Fluo-ST2 (Emulseo, France). The parts were filled with the fluorosilane solution, while the inlet and outlet of the spheroid cultivator was sealed to avoid modification of this area. Then the chip was put on a hot plate tempered at 65 °C and left until the next day.

### 2.3 Droplet Generation, Handling, and Stability Control

For the droplet generation in the cross-junction part of the chip, we used a hydrofluorether HFE-7500 (Emulseo, France) as the continuous phase, with the addition of 1% (w/w) fluorinated surfactant FluoSurf (Emulseo,

France) to keep the aqueous droplets stable for the period of the tumor spheroid formation. To further ensure droplet stability, we have modified the inner surface of the generator and reservoir parts of the system to make it fluorophilic, which helped to prevent the walls from wetting by the aqueous phase in the environment of the HFE-7500. After the spheroids were formed in the aqueous droplets in the droplet reservoir area, we used a 10% (w/w) solution of 1H,1H,2H,2H-Perfluoro-1-octanol (Sigma-Aldrich) in HFE-7500 to coalesce the droplets into continuous aqueous phase, to be able to move the released spheroids oil-free into the cultivation part of the chip.

## 2.4 In Vitro 2D/3D Cell Cultures

### 2.4.1 In Vitro 2D Cell Cultures

Three different model cell lines were used in our experiments. MCF-7 (Human epithelial adenocarcinoma, HTB-22, ATCC) cell line and GAMG (Human glioma, Sigma Aldrich) cell line were cultivated in Dulbecco's Modified Eagle's Medium (DMEM—21063029, Gibco™) supplemented with 10% (v/v) foetal bovine serum (FBS, Sigma-Aldrich), 0.1% (w/v) penicillin, and 0.1% (w/v) streptomycin (Sigma-Aldrich). U87-MG (Human brain glioblastoma, ATCC, HTB-14) cell line was cultivated in Eagle's Minimum Essential Medium (EMEM—M2279-6X1L, Sigma-Aldrich spol. s r.o.) supplemented with 10% (v/v) foetal bovine serum (FBS, Sigma-Aldrich), 0.1% (w/v) penicillin, and 0.1% (w/v) streptomycin (Sigma-Aldrich). All cell lines were maintained in culture flasks with a surface area of 25 cm<sup>2</sup> and a maximum volume of 10 mL. The cell lines were cultivated in the cell culture incubator (Esco Micro Pte. Ltd.) at 37 °C in a humidified atmosphere (95%), including 5% CO<sub>2</sub>. The cell lines were passaged two times per week after achieving 40–60% confluence. After the medium was removed, the flask was rinsed with PBS buffer (Phosphate Buffered Saline, P4417, Sigma-Aldrich spol. s r.o.). Then, trypsin solution (Trypsin–EDTA, T4174, Sigma-Aldrich spol. s r.o., diluted 10×) was added, and cells were incubated for 5 min in the cell incubator. The cells were loosened apart by repeated pipetting in the cell culture medium. The number of cells was determined using trypan blue exclusion on a CellDrop FL (DeNovix Inc.).

### 2.4.2 Formation of 3D Spheroids on Patterned Agarose

The formation of control spheroids was done in MicroTissues 3D Petri Dish micro-mold (Z764051-6EA, Sigma-Aldrich spol. s r.o.). The molds were incubated in 70% ethanol for 30 min and rinsed with ddH<sub>2</sub>O prior to the experiment. The agarose mix consisted of 2 g of agarose (282199, iBioTech) and 100 mL 0.9% NaCl (10020366, Lachema) in ddH<sub>2</sub>O, both autoclaved separately and then mixed together. 370 µL of dissolved agarose has been added to every stamp and left to cool down for 3 min. Patterned agarose was transferred into a 24-well cell culture plate (142485, Trigon plus s.r.o.). For the MCF-7 cell line, Dulbecco's Modified Eagle's Medium/F12 (11320033, Gibco™) mixed with growth factors—20 ng/mL EGF (PHG0315, Gibco™), 20 ng/mL FGF (PHG0264, Gibco™) and 1% B27 (17504044, Gibco™) was added into all wells. For U87-MG and GAMG cell lines, Eagle's Minimum Essential Medium (EMEM—M2279-6X1L, Sigma-Aldrich spol. s r.o.) supplemented with 10% (v/v) foetal bovine serum (FBS, Sigma-Aldrich), 0.1% (w/v) penicillin, and 0.1% (w/v) streptomycin

(Sigma-Aldrich) was used. The plate was then incubated in the cell incubator for 30 min. The medium from each well was later discarded, and 75 µL of the cell suspension of concentration 1,600,000 cells/mL was introduced into each well and incubated for 30 min in the cell incubator. Afterward, 1.5 mL of the cell media was added to each well, and the plate was incubated in the cell incubator for a minimum of 8 h.

## 2.5 OSTE+ Material Influence on Pre-formed 3D Spheroids

In our recent work [22], we have shown that OSTE+ material is practically non-toxic to cell cultures grown as monolayers on this material. To evaluate the suitability of OSTE+ material for 3D spheroid formation, manipulation, and cultivation in microfluidic chip, the behavior and stability of already pre-formed 3D tumor spheroids on OSTE+ polymer surface has been initially tested in this work. For this purpose, we have fabricated OSTE+ polymer pieces and inserted them in conventional well bottoms (for testing of the fluorosilane modification) and further a whole well plate from the OSTE+ polymer (for testing of the Silane-PEG1k-OH modification). Three types of OSTE+ surfaces were tested: (1) modified with Fluo-ST2, (2) modified with Silane-PEG1k-OH and (3) intact OSTE+ polymer. The spheroids created by the conventional method described above were put in each well with a cell culture medium and observed for two days under a confocal microscope.

## 2.6 Microfluidic Chip Experimental Setup, Conditions and Procedure

We worked with 3 switchable outlets [the reservoir main outlet port (9), the reservoir side channel outlet (7) and spheroid cultivator outlet (16)] and 4 inlets [the generator aqueous and oil phase inlets (2, 1), the reservoir side channel inlet (6) and the spheroid cultivator medium inlet (11)] (for clarification, numbers denotes the description of inlets/outlets based on Fig. 1). First, the droplet generator and reservoir parts of the microfluidic chip were filled with HFE-7500 liquid through the oil phase inlet (1) and reservoir side channel inlet (6) and the spheroid cultivation part was filled with isopropanol through the spheroid cultivator medium inlet (11), followed by the aqueous phase (PBS buffer or corresponding cell culture medium) slowly, to prevent the formation and retention of air bubbles. The isopropanol had to be used prior to the aqueous phase in the cultivator because of low wetting of the walls by the aqueous phase, where the water did not enter most of the sieve microchannels when dry due to the capillary repulsive effect. After filling the chip with the

liquids described above, the aqueous phase (cell culture medium) was introduced into the chip through the aqueous phase inlet (2). Initial air bubbles and aqueous droplets were removed from the system by stopping the aqueous phase flow and only keeping the flow of the oil phase, letting them escape through the reservoir outlet (9) while keeping the spheroid cultivator outlet (16) and reservoir side channel outlet (7) closed. In the next step, 500  $\mu\text{L}$  of the prepared cell culture suspension with concentration of 3 million/mL was injected into the aqueous phase inlet (2) with a medical syringe through an injection port (Ibidi). The volume injected was sufficient for the formation of droplet-encapsulated spheroids in the complete volume of the droplet reservoir of the chip. The excess volume of cell suspension (which was pushed into the chip by the syringe) was removed with the same procedure as the initial droplets and bubbles, and after the removal, the oil and aqueous phase (cell culture medium) flow were turned on, resulting in generation of aqueous droplets with the encapsulated cell suspension. The aqueous phase inlet (2) flow rate was set to double of the flow rate of the oil phase (mostly we used 20  $\mu\text{L}/\text{min}$  for the oil phase and 40  $\mu\text{L}/\text{min}$  for the aqueous phase). During the droplet generation, we kept closed the reservoir outlet (9) and opened the side channel outlet (7), causing the oil phase to be pushed away through the branches of this reservoir bottom channel (due to higher density of oil over aqueous phase), while retaining the aqueous droplets in the reservoir until its whole surface area was filled with the droplets. The whole system was kept at 36.5 °C in an incubation box (Okolab), which was a part of the microscope used for observation and data collection. After the formation of the spheroids, the disruption agent solution (10% w/w of 1H,1H,2H,2H-Perfluoro-1-octanol in HFE-7500) was introduced to the chip reservoir area through reservoir side channel inlet (6), with the reservoir side channel outlet (7) opened. Once the droplets were coalesced, additional aqueous phase volume (cell culture medium) was introduced to the chip, at first, from the aqueous phase inlet (2) of the droplet generator and then also from the spheroid cultivator medium inlet (11), until all the aqueous areas were connected (coalesced) and the oil phase flushed out of the chip through the reservoir side channel outlet (7). With all the aqueous areas in the chip connected and oil removed, the transfer of the spheroids to the cultivation part was done by closing the reservoir side channel outlet (7), opening the spheroid cultivator outlet (16), and introducing more cell culture medium through the aqueous phase inlet (2). This pushed the spheroids from the reservoir part into the cultivator, where they could be trapped in its sieve structure. After trapping the spheroids, a new medium

was introduced during the cultivation process through the spheroid cultivator medium inlet (11).

## 2.7 CFD Simulations

The CFD simulations were used to support the design of the spheroid cultivation part of the microfluidic chip and its trapping capability. The mathematical model used considered a steady-state incompressible isothermal flow, which can be described by the conservation equations of mass (the continuity equation) and momentum (the Navier–Stokes equations):

$$\nabla \cdot \mathbf{u} = 0,$$

$$\rho \mathbf{u} \cdot \nabla \mathbf{u} = -\nabla p + \mu \Delta \mathbf{u} + \rho \mathbf{g},$$

where  $\rho$  is density of the fluid,  $\mu$  is its dynamic viscosity,  $\mathbf{u}$  is velocity field vector,  $p$  is pressure,  $\mathbf{g}$  is gravitational acceleration,  $\nabla$  represents nabla operator and  $\Delta$  stands for Laplace operator.

Numerical simulations were performed with open-source software OpenFOAM, using the finite volume method for discretization. The solver chosen for the simulations was simpleFoam. A non-uniform computational grid was used. The number of computational grid cells was approximately  $2.3 \times 10^7$ , and grid refinement was performed near the walls. The following boundary conditions were assumed for the geometry of the cultivator: (i) velocity inlet: the constant value of velocity; (ii) pressure outlet: the constant value of pressure; (iii) walls: no-slip condition.

## 2.8 Data Collection and Evaluation

Tumor spheroids, their formation, and development were imaged on Leica SP8 confocal microscope equipped with an environmental chamber (Okolab) maintaining a stable temperature at 36.5 °C and supplied with humidified air reaching up to 95% RH. The images were taken using HC PL FLUOTAR CS 5  $\times$  /0.15 N.A. dry Leica objective. Leica Las X Navigator function was used for imaging defined areas of the chip. The collected images were further processed with FIJI ImageJ [25].

## 3 Results and Discussion

### 3.1 Advantages of OSTE+ Polymer in Droplet Microfluidics and Spheroid Cultivation

The selection of materials for the fabrication of microfluidic chips, especially those intended for extended cell cultivation, is pivotal to ensure success. Several key aspects need careful

consideration, including biocompatibility, cell adhesion or repellent properties, gas permeation, optical properties, reusability, and fabrication methodologies. Previous studies have primarily utilized PDMS (polydimethylsiloxane), glass, or a combination of both for fabricating droplet microfluidic systems aimed at cell encapsulation and, potentially, tumor spheroid formation [7, 8, 11–13]. However, these materials pose certain limitations in terms of design, prototyping, and fabrication of microfluidic chips. Glass, for example, is not conducive to rapid prototyping and design testing. PDMS, while versatile, presents challenges such as gas permeation, which can impact prolonged cell cultivation and fabrication of complex 3D systems with large surface area. Moreover, PDMS also absorbs various organic solvents, including ethers [23, 24]. This could hamper the long-term on-chip storage of generated water droplets with encapsulated cells in the oil phase (hydrofluoroether), a condition which is needed for initialization of spheroid formation and their later release in water phase. We have confirmed the leakage of hydrofluoroether HFE-7500 from a PDMS channel in a test with a sealed PDMS system that was plasma-bonded to a glass slide, which is the common technique used for PDMS-based microfluidic systems. The leakage through the PDMS was apparent after 5 h, with a complete evaporation of the liquid after 48 h. The test is shown in Fig. S17.

To address these issues, we have chosen OSTE+ (off-stoichiometry thiol-ene epoxy) polymer for our experiments. This material has demonstrated numerous advantages over traditional materials used in microfluidic device prototyping and fabrication. It is characterized by its optical transparency and biocompatibility. Additionally, it undergoes a unique two-step curing process, facilitating soft lithography before hardening. This process also enables permanent bonding to a diverse range of materials. Furthermore, it offers the potential for various surface modifications, such as silanization [19–22].

Prior to developing our devices, we confirmed the suitability of OSTE+ material for droplet microfluidic device fabrication and its compatibility with 3D spheroid cultivation. A crucial factor in our success was the surface modification of OSTE+ using fluorosilane Fluo-ST2 (Emulseo, France) and Silane-PEG-OH (Biopharma PEG Scientific Inc., USA). Our recent work [22] demonstrated through various physico-chemical methods (zeta-potential, XPS, contact angle measurement, etc.) that the fluorosilane permanently modifies the surface of OSTE+, creating a fluorophilic surface essential for stabilizing water–oil (hydrofluoroether) emulsions. Furthermore, we observed limited cell adhesion and low cytotoxicity on these surfaces. Our designed system also includes a spheroid cultivator part, for which we assessed the suitability of silane-modified surfaces in maintaining the 3D structure of pre-formed spheroids (refer to Fig. S11). Without any surface

modification, the spheroids began to disintegrate over the course of cultivation due to preferential cell attachment to the surface. With the fluorosilane modification, although some cells detached from the main spheroid bodies, the spheroids retained their spherical shape with distinct edges. However, after 48 h, there was still significant attachment of the spheroid cells to the surface. With the silane-PEG-OH modification, the anti-fouling properties of the surface were further improved. The spheroids did not show any signs of attachment to the surface and the detached cells from the spheroids were unable to survive or proliferate on the modified surface for an extended period. This led us to conclude that OSTE+ polymer, when modified with Silane-PEG-OH, is well-suited for the construction of the spheroid cultivator part of our system. Another advantage of the OSTE+ material is the re-usability of the fabricated chips. In our experiments, we reused the OSTE+ chips multiple times, maintaining their effectiveness with no aqueous phase wetting of the walls observed for up to five uses. Post-experiment, each chip was thoroughly rinsed and flushed with detergent to remove any residual spheroids, followed by a sonication clean in isopropanol at 50 °C for 15 min. After several cleaning cycles, we noted a reduced functionality of the surface modification, which was readily restored with a new coating. Additionally, the OSTE+ material facilitated the straightforward fabrication of microfluidic devices. This was achieved by fusing two distinctively molded layers, allowing for off-axis channel positioning essential for specific functionalities, such as the aqueous phase inlet (2) and reservoir side channel inlet and outlet (6, 7) (Fig. 2a, b).

### 3.2 Droplet Generation

In our study, we successfully filled the droplet reservoir entirely with a monolayer of droplets. This was accomplished by utilizing the bottom reservoir's side channel (7) as an outlet during the filling process. The reservoir of our final chip model, as depicted in Fig. 1, accommodates approximately 160 aqueous phase droplets, each with a diameter of 800  $\mu\text{m}$ . Our experiments on flow rate impact revealed that droplet size could be finely tuned from 500 to 1000  $\mu\text{m}$ , with a remarkably low size deviation of  $\pm 1\%$ . We observed that the aqueous phase flow rate had a more pronounced effect on droplet size compared to the oil phase flow rate. The droplet diameter increased with the aqueous phase flow rate. This is in contrast to the study by Kwak et al. [14], who used the same oil phase (HFE-7500) and a comparable surfactant, but with the droplet size decreasing under similar conditions. This discrepancy could be due to differences in the water–oil flow ratio, system geometry, or surfactant concentration. Lee et al. [16] regulated droplet size via the oil flow rate, with an increase in flow leading to smaller droplets. We observed a similar but less pronounced trend. Based



on our findings, we opted to regulate droplet size primarily by adjusting the aqueous phase flow rate while keeping the water–oil flow ratio constant. The oil phase flow rate was found to influence both the spacing between droplets and their movement speed. We settled on a water–oil flow ratio of 2:1, which yielded optimal droplet spacing and a manageable flow speed, allowing sufficient time for observation and manipulation of the system. The relationships between the tested flow rates and the resulting droplet diameters are detailed in Fig. 3.

In our cell-based experiments, we chose flow rates of 20  $\mu\text{L}/\text{min}$  for the oil phase and 40  $\mu\text{L}/\text{min}$  for the aqueous

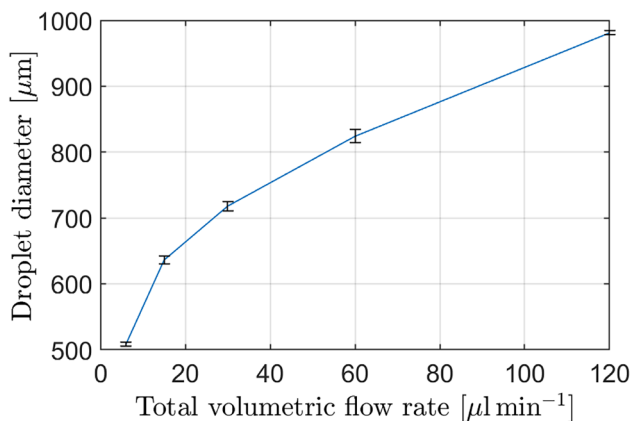


**Fig. 3** Generated droplet sizes based on the flow rates. The water–oil flow ratio was 2:1

phase. This setup yielded droplet diameters just above 800  $\mu\text{m}$ . The larger droplet size was intended to facilitate the formation of bigger spheroids, which are easier to retain in the spheroid cultivation part of our chip. Additionally, these larger droplets provide sufficient nutrients for the spheroids to survive at least 24 h.

### 3.3 Spheroid Formation

#### 3.3.1 Optimization of Cell Count/Droplet Volume Ratio

The primary objective of our study was to achieve the pre-formation of stable, hydrogel-free spheroids within aqueous droplets, enabling their seamless integration into a cell culture medium and further distribution across various sections of a microfluidic chip, all without the need for manual intervention. This approach marks a significant innovation over existing methodologies in this domain, paving the way for the development of high-throughput, automated systems. Central to our success was establishing the ideal ratio of initial cell count to droplet volume. This ratio is crucial for ensuring the viability of the pre-formed spheroids over extended periods (at least 12 h) within the droplets, and for achieving the necessary spheroid integrity and stability for subsequent fluid handling within the chip. To facilitate these optimization studies, we initially developed a microfluidic device featuring a large, oval-shaped droplet reservoir (see Fig. 4). This design provided ample capacity for the droplets, allowing for robust statistical analysis. Efficient optimization

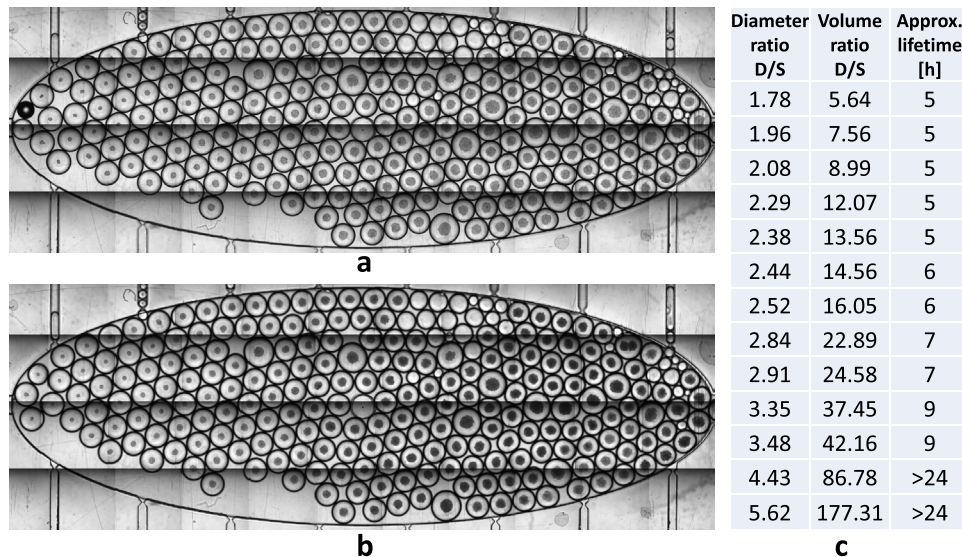


**Fig. 4** A large reservoir chip version, filled with concentration gradient of cells inside the droplets. **a** After 8-h incubation, where spheroids are freshly formed. **b** After 16-h incubation, where the larger spheroids are already dead because of depletion of the nutrients in the droplets, while the smaller spheroids are still alive (the time of

death was determined approximately based on the cessation of movement of the cell aggregates and a color change-from gray to black). **c** A table with representatively selected spheroids across the reservoir length with calculated droplet (D)/spheroid (S) diameter and volume ratios and approximate corresponding lifetimes

was possible within this setup in a single experimental run, assuming the correct selection of the volume of the injected cell suspension and taking into account the dilution effect on the cell concentration towards the end of the injection process. Once we determined the optimal cell-to-volume ratio, maintaining this ratio in the final chip design (illustrated in Figs. 2 and 6) became straightforward. This was achieved by setting the desired cell concentration (based on the predetermined droplet volume and requisite cell count) and ensuring a consistent inflow of the cell suspension into the droplet generator.

Figure 4 presents the results of our optimization study, where cells were introduced into the droplet reservoir following a concentration gradient. At the beginning of incubation, we determined the initial cell count within each droplet, ensuring that individual cells were visible in a single focal plane. We then observed the formation and growth of spheroids during time-lapse cultivation experiments. The lifespan of the pre-formed spheroids within the droplets was inherently limited by nutrient availability, which varied depending on the droplet's size and the initial cell count. Typically, the droplet-to-spheroid volume ratio in our experiments ranged from approximately 5–200, assuming a spherical shape for spheroid volume estimations. A key observation was that higher initial cell counts in the droplets led to quicker nutrient depletion and subsequent spheroid dying out. The end of spheroid viability was approximated by observing the cessation of cellular aggregate movement and a noticeable color shift from gray to black. These indicators of spheroid dying out were previously documented and detailed in our earlier study[26]. We additionally supported this approximation method of spheroid lifetime determination by executing a live/dead assay in microwell plate, comparing the spheroid gray level with the amount of dead cells visible with the assay, which is shown in supplementary, Fig. SI6. Our results suggest that to ensure the survival of pre-formed spheroids for a minimum of 24 h, the cell concentration and droplet size should be calibrated to achieve

a droplet-to-spheroid (D/S) volume ratio of at least 50, or a D/S diameter ratio of 4 or more. Additionally, we noted that excessive cell counts in droplets tended to result in the aggregates adopting a more planar than spherical shape. This deviation in shape can hinder the feasibility of subsequent spheroid manipulations within the microfluidic system.

### 3.3.2 Statistical Analysis of the Spheroid Properties

An additional benefit of our methodology is that it facilitates the automatic acquisition of statistical data pertaining to various parameters, such as the shape of the spheroids, their size, the cell count within droplets, and the droplet size itself. Remarkably, this can be accomplished in a single experimental run. We have initially demonstrated this capability through image analysis, where we evaluated the size distribution of spheroids within droplets and correlated this with the initial cell count for each tested cell line, as depicted in Fig. SI2. It is particularly notable that when an equal number of cells are introduced into the droplet, the spheroids formed from U27 and GAMG cells are consistently larger than those derived from MCF-7 cells. This size difference is observed irrespective of the presence of growth factors.

An additional parameter that can be quantified through image analysis is the acircularity index of spheroids, defined as the ratio of the circumference of the polygon enclosing the shape of the spheroid and the circumference of the circle with the same area as the abovementioned polygon. This index serves as a numerical representation of shape uniformity when viewing the spheroid as a two-dimensional projection. An acircularity index of 1 indicates a perfect circle, with higher values denoting greater deviations from the ideal circular spheroid shape. The acircularity indices for spheroids derived from all tested cell lines are depicted in Fig. SI3 and summarized in Table 1. Data from Fig. SI3 reveal that there is no straightforward correlation between spheroid size and acircularity index. This observation implies that the

**Table 1** Average values of acircularity indexes ( $a$ ), equivalent diameters ( $d_{eq}$ ) for all analyzed spheroids

Cell type	Spheroid formation method	$a$ [-]	$d_{eq}$ [ $\mu\text{m}$ ]
U87	Droplets	$1.22 \pm 0.12$	$373 \pm 43$
	Agarose microwells	$1.23 \pm 0.16$	$188 \pm 39$
MCF + GF	Droplets	$1.21 \pm 0.09$	$182 \pm 29$
	Agarose microwells	$1.14 \pm 0.05$	$169 \pm 31$
MCF NO GF	Droplets	$1.17 \pm 0.10$	$145 \pm 23$
	Agarose microwells	No compact aggregates	
GAMG	Droplets	$1.47 \pm 0.26$	$165 \pm 36$
	Agarose microwells	No compact aggregates	

The MCF-7 cells in the agarose microwells did not form any aggregates without the use of growth factors (GF). The GAMG cells also did not form compact aggregates in the microwells. The source images from which this analysis was done can be found in the supplementary material, Fig. SI4

spheroid's shape (at least in its 2D projection) is influenced more significantly by the cell line type rather than its size, as indicated by the mean acircularity indices in Table 1. The MCF-7 spheroids, cultured without growth factors, exhibited the smallest acircularity values for the droplet method, suggesting a shape closest to a true circle. In contrast, GAMG spheroids displayed a higher acircularity index relative to other cell lines, indicating more pronounced shape variations. However, despite this variability in shape, GAMG spheroids maintained their integrity, moving as cohesive units without disintegrating under fluidic stress.

### 3.3.3 Formation of Spheroids in the Droplets

Utilizing the optimized parameters for spheroid generation, we conducted a subsequent study to evaluate the efficacy of spheroid formation in our microfluidic device compared to the conventional agarose microwell technique (refer to Fig. 5). We aligned the experimental conditions—such as the initial cell count per droplet/well and the volume of the droplet/well—to ensure comparability. Despite these efforts, our observations highlighted notable advantages of the microfluidic system over the standard agarose microwell method in several key aspects. Within our system, all examined cell lines (MCF-7 with and without growth factors, GAMG, and U87 cells) successfully formed stable spheroids within 12 h of incubation. In contrast, the agarose microwell approach failed to yield MCF-7 spheroids in the absence of growth factors, and this limitation was also observed for GAMG cells. While U87 and MCF-7 spheroids (with growth factors) developed in agarose microwells shared similar properties to those formed in droplets, as summarized in Table 1, the formation time in agarose microwells extended to at least 48 h.

In summary, our approach not only facilitates high-throughput spheroid formation and automated statistical analysis but also demonstrates the efficient and rapid production of pre-formed, droplet-encapsulated spheroids. This is notably successful even with cell lines or under conditions where traditional methods are ineffective. Despite the swift advancements in this field, there is a paucity of literature with which to compare the quality and parameters of spheroids generated from identical cell lines using microfluidic techniques. To date, the work of Kwak et al. [14] is the sole study offering a direct comparison, detailing scaffoldless spheroid formation from MCF-7 cell lines using droplet microfluidics. While the spheroid sizes in their study are on par with ours, it remains unclear whether growth factors were employed. Wu et al. [17] managed to produce MCF-7 spheroids of similar dimensions to our own (approximately 100  $\mu\text{m}$ ) in matrigel-supported droplets. However, in the absence of matrigel, their results predominantly featured smaller spheroids and dispersed cells. Lee et al. [16] utilized a methodology similar to that

of Kwak et al. [14] to form U87 spheroids, yielding sizes that were comparable or marginally smaller than those we obtained. A direct comparison of our spheroids with those from studies utilizing hydrogel scaffolds is impracticable. These investigations often involve different cell lines [5, 7, 8, 10, 15] or a combination of cell types [10, 12], which inherently influence the outcome and characteristics of the spheroids.

### 3.4 Release of the Spheroids from Droplets

To enable further manipulation of pre-formed spheroids within the microfluidic chip, a critical additional step involving the coalescence of droplets and the removal of the oil phase was necessary. For this purpose, reservoir side channels (designated as 6 and 7) were employed to introduce a droplet disruption agent, 1H,1H,2H,2H-Perfluoro-1-octanol, into the droplet reservoir. The design of these branched side channels facilitated rapid distribution of the agent throughout the reservoir. This agent, dissolved in the denser HFE phase, flows beneath the droplets as both side channels are positioned at the reservoir's bottom. Additionally, these channels were narrowed at their junctions with the main reservoir to reduce the likelihood of droplets or spheroids being inadvertently forced through.

By flushing approximately 300  $\mu\text{L}$  of a 10% solution of the agent in HFE-7500 through the side branches, we successfully coalesced all aqueous phase droplets, releasing the spheroids into the aqueous medium. This process was completed in under a minute using manual injection with a syringe. Given that the aqueous phase is less dense than the oil phase, it was relatively straightforward to expel the oil phase from the droplet reservoir post-coalescence. This was achieved via the side channels, accompanied by the introduction of an additional culture medium into the chip, as detailed in Sect. 2.6. Consequently, the spheroids suspended in the culture medium could be easily redistributed to other parts of the chip via medium flow. The entire procedure is amenable to automation. Figure 6 illustrates the droplets, both before and after coalescence, containing pre-formed spheroids derived from the MCF-7 cell line.

Our method for the in-chip release of scaffoldless spheroids from droplets represents a novel approach that, to the best of our knowledge, is unique in the field. It paves the way for the development of fully automated systems, eliminating the need for manual handling of spheroids. While Kwak et al. [14] employed the same chemical agent for droplet disruption in HFE-7500, their methodology diverged from ours in significant ways. In their system, spheroid manipulation and the subsequent disruption of aqueous droplets occurred outside the chip, necessitating additional centrifugation steps to isolate the spheroids from the resulting mixture. In contrast, Yoon et al. [12]

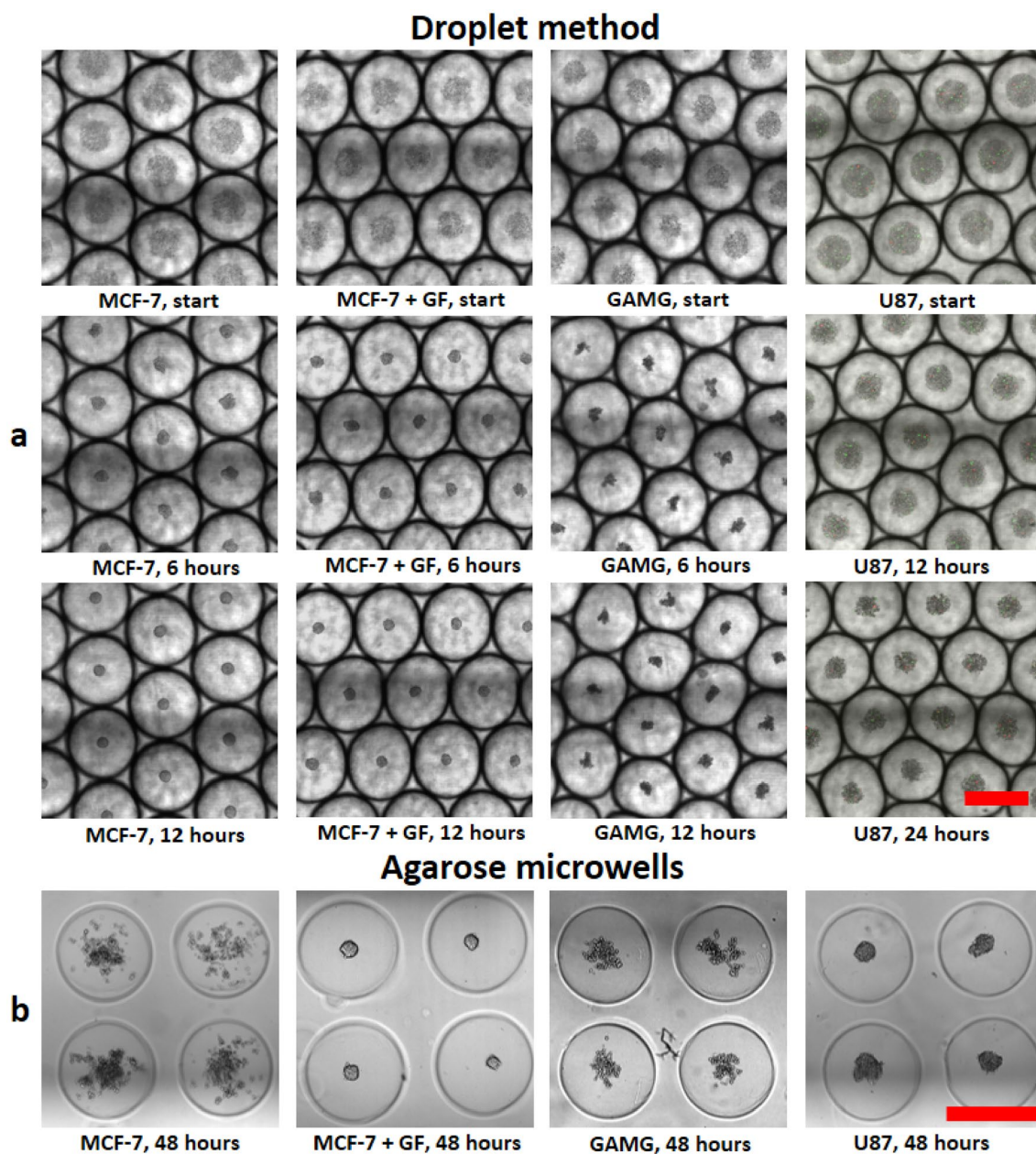
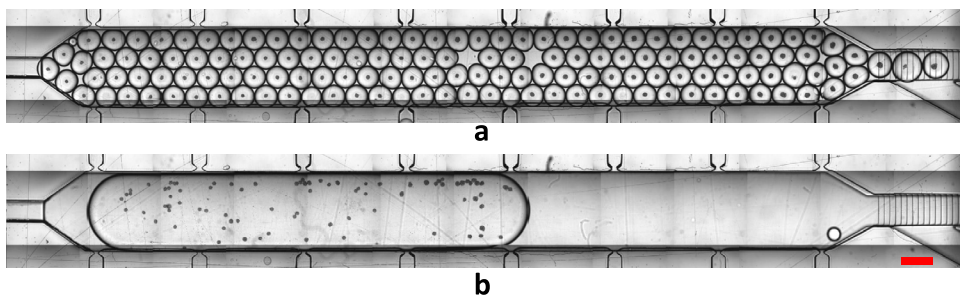


**Fig. 5** Typical cancer spheroids formed from different cell lines in microfluidic chip and agarose microwells. **a** Spheroid formation process with the tested cell cultures inside the microfluidic chip droplet reservoir area. Cell lines and incubation times are listed under each

picture (GF=growth factors). The scale bar is 800 μm for every picture in the droplet method. **b** The appearance of the grown cell cultures after 48 h of incubation in the agarose microwells. The scale bar is 800 μm

**Fig. 6** Reservoir area of the microfluidic chip. **a** Reservoir filled with a monolayer of droplets, each containing a preformed MCF-7 cell line spheroid. **b** Reservoir after introducing the droplet disruption agent, revealing the coalesced aqueous phase with the spheroids. Scale bar: 1200 μm



utilized a magnetic field to extract spheroids from the oil phase, a process that involved the integration of magnetic nanoparticles. However, our chip design circumvents the need for such additives, which could potentially interact with the cells or affect the integrity and formation of the spheroids. Moreover, implementing a magnetic field approach without a hydrogel support structure, which is critical for encapsulating the magnetic nanoparticles, presents its own set of challenges.

### 3.5 Spheroid Trapping and Cultivation System

To showcase the capabilities of our microfluidic system for on-chip formation and distribution of pre-formed spheroids, we have dedicated efforts to developing an integrated spheroid trapping mechanism. The primary objective of this system is to isolate spheroids from the solution, targeting the capture of individual units at specific locations within the chip or trapping system. This setup would facilitate subsequent cultivation and experimental analysis. While our current focus has not been on a specific application, the flexibility of our approach allows for future customizations and modifications to meet diverse on-demand requirements.

#### 3.5.1 Development of Trapping/Cultivation System

Our approach to developing and integrating a spheroid trapping system was twofold: (i) evaluation of existing trapping systems from published studies and (ii) computational fluid dynamics (CFD) modeling coupled with experimental validation of novel systems designed by us (see Fig. 7). Initially, we experimented with a basic obstacle-based trapping system akin to the one described by Yu et al. [11]. However, this method proved ineffective for our spheroids. Unlike larger or more momentum-bearing particles, such as those used by Yu et al. [11], which involved hydrogel encapsulation leading to larger and heavier objects, our scaffoldless spheroids had insufficient momentum. As a result, they easily bypassed the obstacles by following the path of least resistance.

Consequently, our focus shifted to developing a sieve-like structure for effective spheroid trapping. Our initial step involved modifying a design previously published by Jackson et al. [27], which featured inlet and outlet channels on the sides (as shown in Fig. 7a). Despite achieving relatively uniform flow rates through the microchannels with this sieve design, we encountered a significant challenge in trapping the spheroids. The primary issue was the disproportionate flow strength in the main channel, running perpendicular to the sieve's microchannels. This flow was overpoweringly strong compared to the suction into the microchannels, resulting in the spheroids being carried downstream to the right side of the sieve before they could be captured in the chambers situated at the microchannels' entrances.

The spheroids tended to roll over these entry points without being captured inside. As a result, they accumulated at the right end of the sieve, leading to a bottleneck in the trapping process.

In response to these challenges, we designed an alternative system with central inlet and outlet ports in the trapping mechanism (as depicted in Fig. 7b, c). This configuration effectively divided the main flow into two streams, halving the velocity magnitude and thereby enabling the spheroids to access the trapping chambers. While this design showed some promise, as indicated by our computational fluid dynamics (CFD) simulations, the flow predominantly passed through the central microchannels. This issue persisted despite our efforts to elongate these channels to redirect the flow towards the sieve's peripheries (Fig. 7b). To further address this flow imbalance, we modified the height of the individual microchannels from initial 600  $\mu\text{m}$  to final 200  $\mu\text{m}$ . This resulted in a marked improvement in flow distribution, particularly enhancing flow through the outermost parts of the sieve (Fig. 7c). However, the continued refinement of this sieve structure, while important, was outside the scope of our current study and is earmarked as a key area for future research.

#### 3.5.2 Experimental Verification of Spheroid Trapping Mechanism

To streamline development, we initially constructed the trapping and cultivation system as a standalone module separate from the main microfluidic chip. This allowed us to test its effectiveness both in the trapping process and for the extended cultivation of pre-formed MCF-7 spheroids (illustrated in Fig. 8). Following successful optimization, this system was then fully integrated into the microfluidic chip.

The final design of the spheroid trapping and cultivating section (Fig. 7c) proved to be quite effective. We would like to stress that our primary intent was not to achieve a complete occupation of all chambers present in the cultivator part with individual spheroids, but rather to avoid the situation of multiple spheroids in one chamber. From this point of view, the system worked with relative success when the size of the spheroids was comparable to the size of the chambers, showing only 10% or less chambers occupied by multiple spheroids (Fig. 7d - 40 spheroids total, 4 chambers contained multiple spheroids and S15 - 23 spheroids total, one chamber contained 2 spheroids). The trapping process was largely unaffected by variations in flow rate. When a chamber captured a spheroid, the reduced fluid flow through that particular chamber decreased the likelihood of subsequent spheroids being drawn into it, thereby directing them toward empty chambers instead. Despite the simulations (Fig. 7c) showing the largest flow rate in the central part of the cultivator, the distribution of the trapped

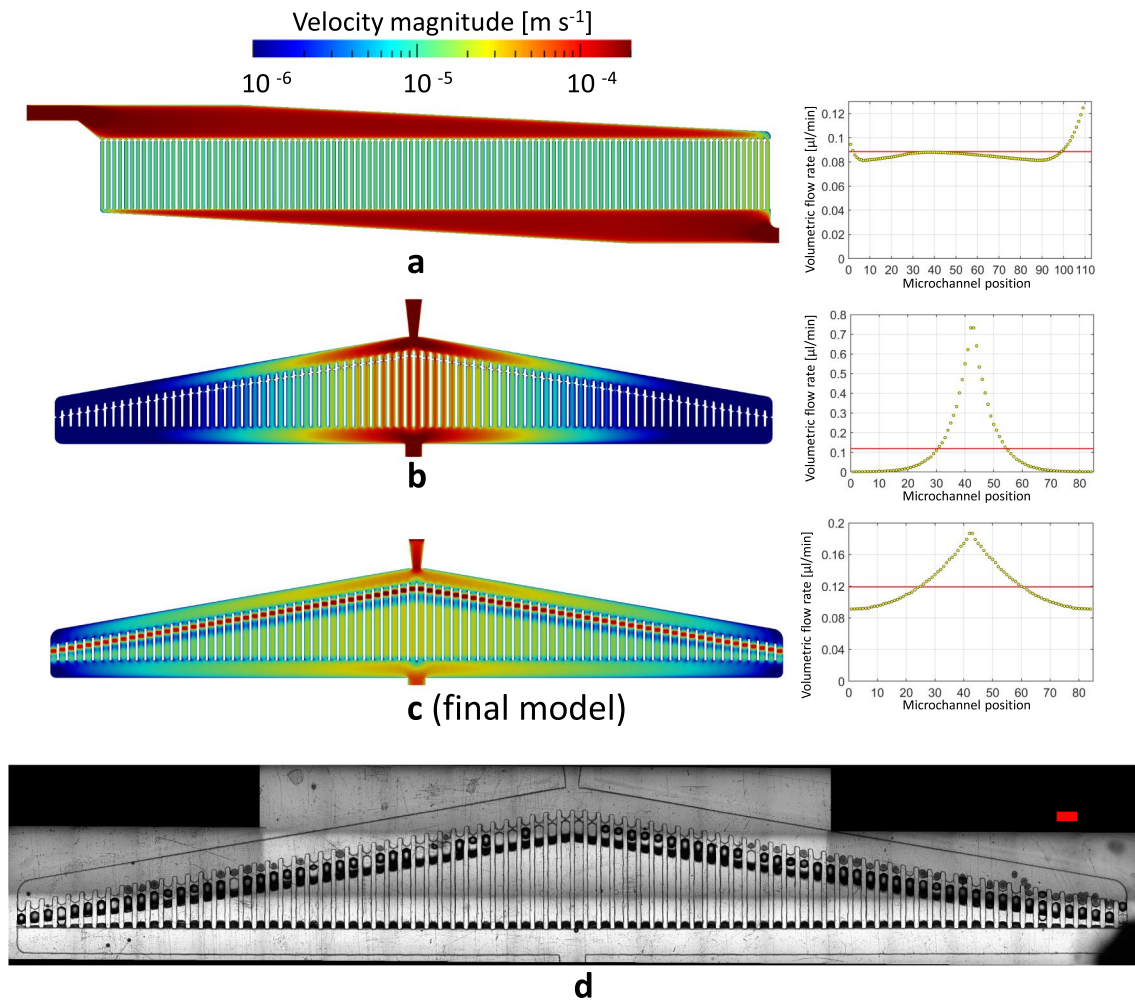


**Fig. 7** Computational fluid dynamics simulation and experimental validation of the spheroid trapping/cultivation system. Panels **a–c** provide an overview of the simulated flow velocity distribution within the spheroid trapping/cultivation section. On the left side of each panel are graphical illustrations of the flow, while on the right side are the volume flow rates through individual microchannels. Panels **a** and **b** showcase the developmental models, with **c** depicting the final, experimentally tested model. The preset volumetric flow rate at the

cultivator's inlet was fixed at  $10 \mu\text{L}/\text{min}$ . In the accompanying graphs, the red line indicates the average flow rate (total flow rate divided by the number of microchannels), and the yellow points represent the flow rates in each microchannel. The graphical illustrations correspond to a plane at a height of  $100 \mu\text{m}$  for panel **a**,  $300 \mu\text{m}$  for panel **b** and  $25 \mu\text{m}$  for **c**. Panel **d** illustrates the trapped spheroids in the final geometry (scale bar: 1 mm)

spheroids (illustrated in Fig. 7d and SI5) was more in favor of the side areas. This was most likely caused by the initial high flow rate in the main channel compared to the flow into individual chambers, similarly as in our previous sieve model (Fig. 7a).

We additionally demonstrated the possibility of extended cultivation of trapped spheroids in perfusion mode. Once ensnared in the trap, the spheroids could be successfully maintained for prolonged periods (at least 5 days), as shown in Fig. 8. The cultivation conditions were set to deliver  $10 \mu\text{L}$  of medium every 150 s to the cultivator inlet. After 118 h, the cultivator was flushed with CellTox Green (Promega, USA)  $2\times$  solution in cell medium for 1 h with flow rate of  $1 \mu\text{L}/\text{s}$ . This substance stains dead cells by binding to DNA

and forming a fluorescent complex with it (excitation peak 513 nm, 488 nm argon laser was used, emission 532 nm). The substance cannot penetrate living cell membranes and will thus only stain dead cells. It will also not penetrate into and stain the spheroid necrotic cores. Throughout the cultivation period, the spheroids retained their shape without any noticeable disintegration. After 96 h, we can notice that some cells detached from the spheroid bodies and stayed in the microchannels behind. Part of those cells were still alive, as can be seen from the 118-h image. At the end of the cultivation, we can see that part of the cells on the spheroid surfaces are dead, which was probably caused by insufficient flow rate during the cultivation. However, the spheroids still retained their integrity and majority of live cells.

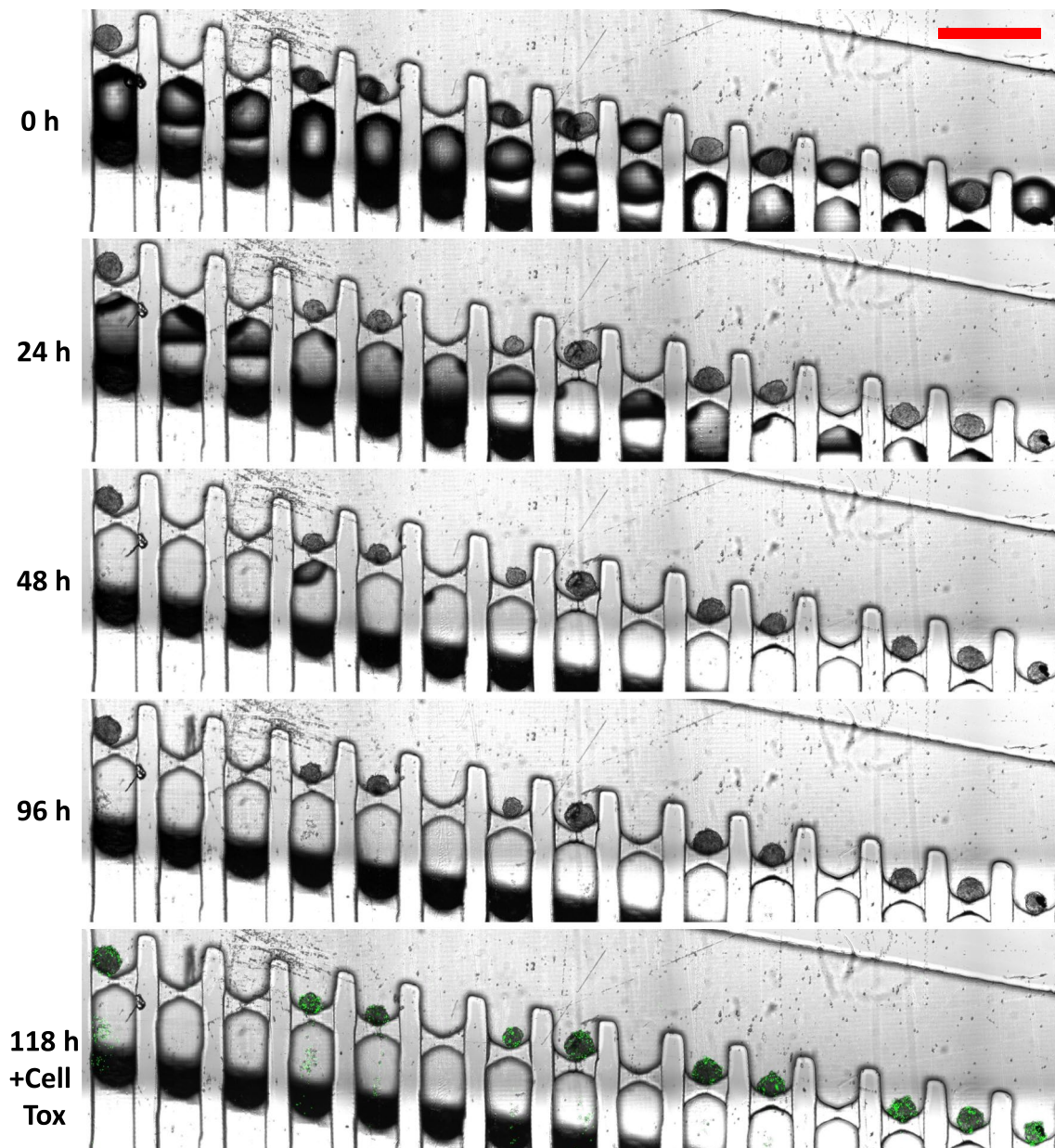


**Fig. 8** Close-up of the cultivation area with trapped MCF-7 cell spheroids. These spheroids were formed by the patterned agarose method and were 24 h old when put into the chip. After 118 h, the spheroids were stained with CellTox Green to detect dead cells. The fluorescent

image was compiled from z-stacks with maximum intensity on a confocal microscope and represents fluorescence from the whole spheroid surface. The scale bar is 1 mm

To further demonstrate the OSTE+ polymer compatibility with fluorescent imaging, we have formed spheroids from GFP-transfected U-87 cells (in agarose microwells) and trapped them in the chip cultivator. One cell line was transfected with EGFP (excitation 488 nm, emission 507 nm) and the second one with mScarlet-I (excitation 569 nm, emission 593 nm). The spheroids were cultivated for 24 h and their fluorescence was observable without any visible background from the OSTE+ polymer (Fig. S15).

## 4 Conclusions

In the dynamic field of cancer research, the shift towards 3D cell cultures, particularly tumor cell spheroids, marks a significant advancement in replicating the complexity of in vivo tumor microenvironments. Tumor spheroids are valued for their ability to better mimic the cellular architecture and drug response characteristics of real tumors, especially in the context of drug resistance. Traditional 2D cultures fall short in this aspect, often leading to misleading

drug efficacy results due to their oversimplified nature. A notable challenge in leveraging these 3D cultures is the consistent formation of uniform spheroids and their precise manipulation for drug screening. Uniformity in size and shape is crucial for reliable results, but achieving this has been a complex hurdle in the field.

Our study addresses this challenge by introducing a novel microfluidic system that utilizes droplet microfluidics for generating uniform, scaffoldless 3D cell cultures (spheroids), with an emphasis on complete in-chip handling. We developed a microfluidic chip comprising integrated droplet generator, reservoir, and cultivation sections, functioning as an integrated system. It streamlines the entire cultivation process by (i) generating tumor spheroids from cell suspensions within individual droplets, (ii) merging these droplets into a continuous aqueous phase upon completion of spheroid formation, and (iii) transferring the spheroids to a specialized area within the chip for extended cultivation. This integrated approach eliminates the need for external handling or hydrogel encapsulation, a common requirement in other methods, thus reducing contamination risks and simplifying the process. The chip was fabricated from OSTE+ (off-stoichiometry thiol-ene epoxy) polymer, known for its robustness and suitability for repeated use. We further demonstrated the system's effectiveness by successfully forming spheroids from various cell lines, including MCF-7, GAMG, and U87. Tumor spheroids were not only formed but also released from droplets and trapped for further cultivation within the chip, showcasing the system's ability to handle delicate processes internally.

We may conclude that our novel microfluidic approach offers a promising avenue for improving high-throughput, automated procedures in the formation, transfer, and cultivation of tumor cell spheroids. This advancement could significantly enhance the accuracy and efficiency of drug screening processes, ultimately accelerating the development of more effective cancer treatments.

**Supplementary Information** The online version contains supplementary material available at <https://doi.org/10.1007/s13206-024-00167-x>.

**Acknowledgements** The authors acknowledge the assistance provided by the Research Infrastructure NanoEnviCz (Project No. LM2018124) and the project Pro-NanoEnviCz (Reg. No. CZ.02.1.01/0.0/0.0/16\_013/0001821 and CZ.02.1.01/0.0/0.0/18\_046/0015586), supported by the Ministry of Education, Youth and Sports of the Czech Republic and the European Union European Structural and Investments Funds in the frame of the Operational Programme Research Development and Education, the ERDF/ESF project “UniQSurf—Centre of biointerfaces and hybrid functional materials” (No. CZ.02.1.01/0.0/0.0/17\_048/007411). This project is also supported by the Internal Grant Agency of Jan Evangelista Purkyně University in Ústí nad Labem (project UJEP-SGS-2023-53-005-3).

**Author contributions** Methodology: PP, JS, MŠ, JH, JM; Investigation: PP, JS, ZŽ, KŠ, VH, PA; Resources: JM, JH; Formal analysis: PP, JS,

MŠ, SV, VH; Writing Original Draft: PP, VH; Writing—Review & Editing: JM, JH, MŠ; Funding Acquisition: JM, JH; Supervision: JM.

**Funding** Open access publishing supported by the National Technical Library in Prague. We have no relevant financial or non-financial competing interests to disclose.

**Data availability** The data that support the findings of this study are available from the corresponding authors, [PP, JM], upon request.

## Declarations

**Conflict of interest** There are no conflicts of interest to declare.

**Open Access** This article is licensed under a Creative Commons Attribution 4.0 International License, which permits use, sharing, adaptation, distribution and reproduction in any medium or format, as long as you give appropriate credit to the original author(s) and the source, provide a link to the Creative Commons licence, and indicate if changes were made. The images or other third party material in this article are included in the article's Creative Commons licence, unless indicated otherwise in a credit line to the material. If material is not included in the article's Creative Commons licence and your intended use is not permitted by statutory regulation or exceeds the permitted use, you will need to obtain permission directly from the copyright holder. To view a copy of this licence, visit <http://creativecommons.org/licenses/by/4.0/>.

## References

1. Siegel, R.L., Miller, K.D., Fuchs, H.E., Jemal, A.: Cancer statistics, 2022. *CA Cancer J. Clin.* (2022). <https://doi.org/10.3322/caac.21708>
2. Rodrigues, T., Kundu, B., Silva-Correia, J., Kundu, S.C., Oliveira, J.M., Reis, R.L., Correló, V.M.: Emerging tumor spheroids technologies for 3D in vitro cancer modeling. *Pharmacol. Ther.* (2018). <https://doi.org/10.1016/j.pharmthera.2017.10.018>
3. Sant, S., Johnston, P.A.: The production of 3D tumor spheroids for cancer drug discovery. *Drug Discov. Today Technol.* (2017). <https://doi.org/10.1016/j.dttec.2017.03.002>
4. Costa, E.C., Moreira, A.F., de Melo-Diogo, D., Gaspar, V.M., Carvalho, M.P., Correia, I.J.: 3D tumor spheroids: an overview on the tools and techniques used for their analysis. *Biotechnol. Adv.* (2016). <https://doi.org/10.1016/j.biotechadv.2016.11.002>
5. Ryu, N.E., Lee, S.H., Park, H.: Spheroid culture system methods and applications for mesenchymal stem cells. *Cells* (2019). <https://doi.org/10.3390/cells8121620>
6. Achilli, T.M., Meyer, J., Morgan, J.R.: Advances in the formation, use and understanding of multi-cellular spheroids. *Expert Opin. Biol. Ther.* (2012). <https://doi.org/10.1517/14712598.2012.707181>
7. Kim, C.: Droplet-based microfluidics for making uniform-sized cellular spheroids in alginate beads with the regulation of encapsulated cell number. *Biochip J.* (2015). <https://doi.org/10.1007/s13206-015-9203-6>
8. Cui, X., Liu, Y., Hartanto, Y., Bi, J., Dai, S., Zhang, H.: Multi-cellular spheroids formation and recovery in microfluidics-generated thermoresponsive microgel droplets. *Colloids Interface Sci. Commun.* (2016). <https://doi.org/10.1016/j.colcom.2016.09.001>
9. Liu, H.T., Wang, H., Wei, W.B., Liu, H., Jiang, L., Qin, J.H.: A microfluidic strategy for controllable generation of



- water-in-water droplets as biocompatible microcarriers. *Small* (2018). <https://doi.org/10.1002/sml.201801095>
10. Sun, Q., Tan, S.H., Chen, Q., Ran, R., Hui, Y., Chen, D., Zhao, C.X.: Microfluidic formation of coculture tumor spheroids with stromal cells as a novel 3D tumor model for drug testing. *ACS Biomater. Sci. Eng.* (2018). <https://doi.org/10.1021/acsbomaterials.8b00904>
  11. Yu, L., Chen, M.C.W., Cheung, K.C.: Droplet-based microfluidic system for multicellular tumor spheroid formation and anticancer drug testing. *Lab Chip* (2010). <https://doi.org/10.1039/c004590j>
  12. Yoon, S., Kim, J.A., Lee, S.H., Kim, M., Park, T.H.: Droplet-based microfluidic system to form and separate multicellular spheroids using magnetic nanoparticles. *Lab Chip* (2013). <https://doi.org/10.1039/c3lc41322e>
  13. Sabhachandani, P., Motwani, V., Cohen, N., Sarkar, S., Torchilin, V., Konry, T.: Generation and functional assessment of 3D multicellular spheroids in droplet based microfluidics platform. *Lab Chip* (2016). <https://doi.org/10.1039/c5lc01139f>
  14. Kwak, B., Lee, Y., Lee, J., Lee, S., Lim, J.: Mass fabrication of uniform sized 3D tumor spheroid using high-throughput microfluidic system. *J. Controll. Release* (2018). <https://doi.org/10.1016/j.jconrel.2018.02.029>
  15. De Lora, J.A., Fencel, F.A., MacÍas Gonzalez, A.D.Y., Bandegi, A., Foudazi, R., Lopez, G.P., Shreve, A.P., Carroll, N.J.: Oil-free acoustofluidic droplet generation for multicellular tumor spheroid culture. *ACS Appl. Bio Mater.* (2019). <https://doi.org/10.1021/acsbam.9b00617>
  16. Lee, J.M., Choi, J.W., Ahrberg, C.D., Choi, H.W., Ha, J.H., Mun, S.G., Mo, S.J., Chung, B.G.: Generation of tumor spheroids using a droplet-based microfluidic device for photothermal therapy. *Microsyst. Nanoeng.* (2020). <https://doi.org/10.1038/s41378-020-0167-x>
  17. Wu, Z., Gong, Z., Ao, Z., Xu, J., Cai, H., Muhsen, M., Heaps, S., Bondesson, M., Guo, S., Guo, F.: Rapid microfluidic formation of uniform patient-derived breast tumor spheroids. *ACS Appl. Bio Mater.* (2020). <https://doi.org/10.1021/acsbam.0c00768>
  18. Zhang, T., Zhang, H., Zhou, W., Jiang, K., Liu, C., Wang, R., Zhou, Y., Zhang, Z., Mei, Q., Dong, W.F., Sun, M., Li, H.: One-step generation and purification of cell-encapsulated hydrogel microsphere with an easily assembled microfluidic device. *Front Bioeng. Biotechnol.* (2022). <https://doi.org/10.3389/fbioe.2021.816089>
  19. Carlborg, C.F., Haraldsson, T., Öberg, K., Malkoch, M., Van Der Wijngaart, W.: Beyond PDMS: off-stoichiometry thiol-ene (OSTE) based soft lithography for rapid prototyping of microfluidic devices. *Lab Chip* (2011). <https://doi.org/10.1039/c1lc20388f>
  20. Sticker, D., Geczy, R., Häfeli, U.O., Kutter, J.P.: Thiol-ene based polymers as versatile materials for microfluidic devices for life sciences applications. *ACS Appl. Mater. Interfaces* (2020). <https://doi.org/10.1021/acscami.9b22050>
  21. Sticker, D., Rothbauer, M., Lechner, S., Hehenberger, M.-T., Ertl, P.: Multi-layered, membrane-integrated microfluidics based on replica molding of a thiol-ene epoxy thermoset for organ-on-a-chip applications. *Lab Chip* **15**, 4542–4554 (2015). <https://doi.org/10.1039/C5LC01028D>
  22. Aubrecht, P., Smejkal, J., Panuška, P., Španbauerová, K., Neubertová, V., Kaule, P., Matoušek, J., Vinopal, S., Liegertová, M., Štofík, M., Malý, J.: Performance and biocompatibility of OSTEMER 322 in cell-based microfluidic applications. *RSC Adv.* **14**(6), 3617–3635 (2024). <https://doi.org/10.1039/d3ra05789e>
  23. Vinothkumar, T., Arathi, G., Kandaswamy, D., Dinesh, K.: Influence of different organic solvents on degree of swelling of poly(dimethyl siloxane)-based sealer. *J. Conserv. Dent.* **14**(2), 156 (2011). <https://doi.org/10.4103/0972-0707.82621>
  24. Lee, J.N., Park, C., Whitesides, G.M.: Solvent compatibility of poly(dimethylsiloxane)-based microfluidic devices. *Anal. Chem.* **75**(23), 6544–6554 (2003). <https://doi.org/10.1021/ac0346712>
  25. Schindelin, J., Arganda-Carreras, I., Frise, E., Kaynig, V., Longair, M., Pietzsch, T., Preibisch, S., Rueden, C., Saalfeld, S., Schmid, B., Tinevez, J.Y., White, D.J., Hartenstein, V., Eliceiri, K., Tomancak, P., Cardona, A.: Fiji: an open-source platform for biological-image analysis. *Nat. Methods* (2012). <https://doi.org/10.1038/nmeth.2019>
  26. Žmudová, Z., Šanderová, M., Liegertová, M., Vinopal, S., Herma, R., Sušický, L., Müllerová, M., Strašák, T., Malý, J.: Biodistribution and toxicity assessment of methoxyphenyl phosphonium carbosilane dendrimers in 2D and 3D cell cultures of human cancer cells and zebrafish embryos. *Sci. Rep.* (2023). <https://doi.org/10.1038/s41598-023-42850-3>
  27. Jackson, J.M., Hupert, M.L., Soper, S.A.: Discrete geometry optimization for reducing flow non-uniformity, asymmetry, and parasitic minor loss pressure drops in Z-type configurations of fuel cells. *J. Power. Sources* (2014). <https://doi.org/10.1016/j.jpowsour.2014.06.136>

**Publisher's Note** Springer Nature remains neutral with regard to jurisdictional claims in published maps and institutional affiliations.